DOI: 10.1070/RCR4907

Resonant tunnelling spectroscopy of van der Waals heterosystems

Evgenii E. Vdovin,[a] Konstantin S. Novoselov,[b] Yurii N. Khanin [a]

[a] Institute of Microelectronics Technology and High Purity Materials, Russian Academy of Sciences, ul. Osipyana 6, 142432 Chernogolovka, Moscow Region, Russian Federation
[b] School of Physics and Astronomy, University of Manchester, Oxford Road, M13 9PL Manchester, United Kingdom

The review concerns the most interesting aspects of (mainly experimental) resonance tunnelling spectroscopy studies of a new type of heterosystems called van der Waals heterostructures. The possibility to compose such systems is a result of the recent discovery of two-dimensional crystals, a new class of materials derived from graphene. The role of the angular mismatch of the crystal lattices of conductive graphene electrodes in the tunnelling of charge carriers between them, as well as the closely related issues associated with fulfillment of the conservation laws during tunnelling transitions are considered. The experimental results on inelastic tunnelling in the graphene/h-BN/graphene heterosystems with strong angular mismatch are discussed. The experiments made it possible to determine the phonon density of states spectra of the constituent layers and to detect and describe tunnelling transitions involving localized states of structural defects in the h-BN barrier. We consider new results of studies on tunnelling and magnetotunnelling in van der Waals heterosystems that demonstrate the possibilities of practical application of resonant tunnelling effects in, *e.g.*, microwave engineering, based on realization of electronic devices having $I-V$ curves with negative differential conductance (NDC) regions at tunnelling through defect levels of the barrier layers in such systems. These studies revealed two new types of heterosystems characterized by the formation of NDC regions as a result of resonant tunnelling through the defect levels in the h-BN barrier and by defect-assisted generation of tunnelling current.
The bibliography includes 40 references.

Contents

1. Introduction 1081
2. Tunnelling without momentum conservation in van der Waals heterostructures with arbitrary angular orientation of layers. A field-effect tunnelling transistor based on a vertical structure composed of two graphene layers separated by a dielectric 1083
3. Tunnelling with momentum conservation in van der Waals heterostructures with small angular mismatch of constituent layers 1089
4. Van der Waals heterostructures in a magnetic field perpendicular to layers. Tunnelling transitions between Landau levels in graphene layers 1090

E.E.Vdovin. Candidate of Sciences (Physics and Mathematics), Leading Researcher at the Institute of Microelectronics Technology and High Purity Materials, RAS.
Telephone: +7(496)524 – 4011, e-mail: vdov62@yandex.ru
K.S.Novoselov. Candidate of Sciences (Physics and Mathematics), Professor at Manchester University.
E-mail: kostya@manchester.ac.uk
Yu.N.Khanin. Candidate of Sciences (Physics and Mathematics), Leading Researcher at the Institute of Microelectronics Technology and High Purity Materials, RAS.
Telephone: +7(496)524 – 4027, e-mail: khanin@iptm.ru
Current research interests of the authors: semiconductor physics, nano- and microstructures, two-dimensional crystals, graphene, van der Waals heterostructures.

Received 26 June 2019
Translation: A.M.Raevskiy

1. Introduction

Two-dimensional (2D) layered crystals became the focus of interest of researchers working in the field of design of advanced materials just over ten years ago, following the discovery of graphene (Gr). In 2D crystals, each layer is formed using covalent bonds and held together with adjacent layers through weak van der Waals interactions. This opens up the possibility of separating individual atomic layers of various materials and then combining them with one another to compose diverse van der Waals heterostructures without the need to match the lattice constants of adjacent layers and thus significantly limit the potential of design of conventional epitaxial heterosystems. A van der Waals heterostructure can be composed of dielectric, conductive, superconducting and magnetic layers. Its properties

© 2019 Uspekhi Khimii, Russian Academy of Sciences and Turpion Ltd.

depend on the stacking order of the layers and can be varied with ease. Since there is a wide variety of initial 2D crystals, van der Waals heterostructures can exhibit certain combinations of physical properties which previously could not be imagined; this makes it possible to design novel electronic devices with unique properties and functional characteristics.

Resonant tunnelling spectroscopy has long proved itself as reliable, highly sensitive and versatile method of investigation of the properties of semiconductor heterosystems and various quantum mechanical phenomena in them. A huge number of resonant tunnelling spectroscopy studies are available. In this review we will consider publications concerned with the most interesting, from out point of view, and useful information.[1–10] Of course, the design of a novel class of 2D materials whose electronic spectra are atypical of semiconductors (more exactly, realization of van der Waals heterostructures based on 2D crystals) makes resonant tunnelling spectroscopy in high demand.

Prior to reviewing studies on tunnelling in van der Waals heterostructures, we will briefly outline the physical properties of 2D crystals taking the parent compound, graphene, as an example.[11] The 2D hexagonal crystal lattice of graphene can be represented as a combination of two superimposed Bravais lattices with parallelogram-shaped unit cells. The total wave function of electrons in such a crystal can be represented as a linear combination of the wave functions of electrons from different sublattices. Usually, an additional quantum number called pseudospin is introduced to describe this situation. The pseudospin is unrelated to the electron spin, being an index characterizing the contributions of two sublattices to the formation of the total two-component wave function of electrons. The two-component description of charge carriers in graphene is similar to that used in quantum electrodynamics where the spinor wave functions are introduced. In the case of graphene, the spin index specifies membership of an electron in one out of two sublattices and is therefore called pseudospin[11] rather than corresponds to conventional electron spin.

The charge carrier spectrum in graphene is such that the electron and hole bands contact each other at the corners of the hexagonal Brillouin zone. The carriers responsible for the conductance of undoped graphene are localized at just these six contact points. There are two independent branches of the spectrum in the Brillouin zone, each of them having the form

$$E = \hbar \upsilon_F \boldsymbol{k}, \quad (1)$$

where the wave vector $\boldsymbol{k}$ is measured from the contact point and the velocity of an electron at the Fermi level (Fermi velocity) υ_F is of the order of 10^8 cm s^{-1}. This is the so-called massless spectrum and the corresponding charge carriers are described by the Dirac equation. Besides, graphene is a two-valley semimetal, *i.e.*, it is sufficient to consider only two adjacent corners in the hexagonal Brillouin zone in order to describe the carrier states, and the Dirac equation should be modified to take account of electrons and holes from different valleys (K, K').

Presentation of material in this review mainly follows the history of upgrading of van der Waals heterostructures from systems with randomly oriented conductive and barrier layers to well-matched ones (angular lattice mismatch less than 2°) and then to studies of the influence of controlled misorientation on the properties of the structures in question. In conclusion, we will briefly outline new potential fields of practical application of the results of research into resonant tunnelling effects in van der Waals heterostructures. Examples considered below include the studies that reported different methods for realization of negative differential conductance (NDC) regions in the $I-V$ curves, which are due to tunnelling transitions involving localized defect states in hexagonal boron nitride (h-BN) barrier layers. The existence of the NDC regions in different systems attracts constant attention of researchers in connection with the need for various nanoelectronics devices, such as microwave oscillators, logic gates and functional units for quantum computing systems. As to the graphene van der Waals heterosystems, such studies are extremely topical[12] since they assume the possibility to generate frequencies up to the terahertz range[13] and demonstrate feasibility of the NDC regions. In addition, the authors of a study[14] of tunnelling and magnetotunnelling through a h-BN barrier separating graphene layers with well-matched crystal lattices (small angular mismatch of the crystal lattices) observed both the NDC region and corresponding generation of tunnelling current.

Notations are as follows:

B — magnetic field,
d — thickness of tunnelling barrier,
DoS_i — density of states in ith layer,
$\mathrm{d}I/\mathrm{d}V_b$ — conductance,
E — energy,
$E_{\mathrm{LO\ phonon}}$ — optical phonon energy,
e — electron charge,
ε — dielectric permitivity,
ε_0 — absolute dielectric permittivity,
F — electric field,
$f(E)$ — Fermi distribution function,
Gr — graphene,
h-BN — hexagonal boron nitride,
$\hbar = h/2\pi$ — Planck constant,
I — electric current,
$I-V_b$ — tunnelling characteristic,
$\boldsymbol{k}$ — wave vector,
μ_b — chemical potential in lower graphene layer,
μ_t — chemical potential in upper graphene layer,
NDC — negative differential conductance,
n_b — carrier concentration in lower graphene electrode,
n_t — carrier concentration in upper graphene electrode,
T — temperature,
υ_F — velocity of an electron at the Fermi level (Fermi velocity),
V_g — gate voltage of transistor structure,
V_{tg} — upper gate voltage of transistor structure,
V_{bg} — lower gate voltage of transistor structure,
V_b — bias voltage between drain and source of transistor structure.

2. Tunnelling without momentum conservation in van der Waals heterostructures with arbitrary angular orientation of layers. A field-effect tunnelling transistor based on a vertical structure composed of two graphene layers separated by a dielectric

Pioneering attempts aimed to fabricate multilayer vertical van der Waals heterostructures were made without understanding the important role of the influence of angular lattice mismatch between the conductive layers of graphene on the interlayer tunnelling conductance; the structures were assembled using graphene flakes with random orientations relative to one another. The most important result of the pioneering studies was the fabrication of a tunnelling field-effect transistor based on heterosystems composed of two mechanically exfoliated graphene layers separated by atomically thin h-BN or MoS_2 barriers. The heterosystem was placed on a heavily doped oxidized silicon Si/SiO_2 substrate acting as a gate.[15] The conductance ratios between the open- and closed-state graphene layers in such transistors were 50 and 10^4, respectively, which suggests the possibility of practical application of the devices (for planar graphene systems, this was impossible because of the absence of a band gap in graphene).

A schematic and optical micrograph of a typical experimental heterostructure Gr/h-BN/Gr, the $I-V$ curves and a schematic description of the influence of the gate voltage (V_g) on the bias voltage between the drain and source (V_b) are presented in Fig. 1. The schematic (see Fig. 1 *a*) also shows an additional thick h-BN layer that was used to increase the charge carrier mobility in graphene sheets (this layer was not mentioned above). Experimental structures are usually covered with an h-BN layer (encapsulated) to protect from atmospheric effects since graphene is extremely sensitive to chemical doping.

The tunnelling $I-V_b$ characteristics (see Fig. 1 *c*) represent exponential curves that are due to electron tunnelling transitions from filled to empty states of the Dirac cones in the upper and lower graphene layers without conservation of the momentum component aligned with the layers, as shown in Fig. 1 *d*. Owing to low density of states near the Dirac point, which is also the electrical neutrality point, the Fermi level can be controlled over a wide range using an external gate. Even at fixed interlayer bias voltage, by increasing and decreasing the Fermi level of graphene electrode layers, by varying the voltage at the outer gate, one can efficiently control the number of filled cathodic and accessible anodic electronic states for tunnelling and, hence, the interlayer tunnelling current.

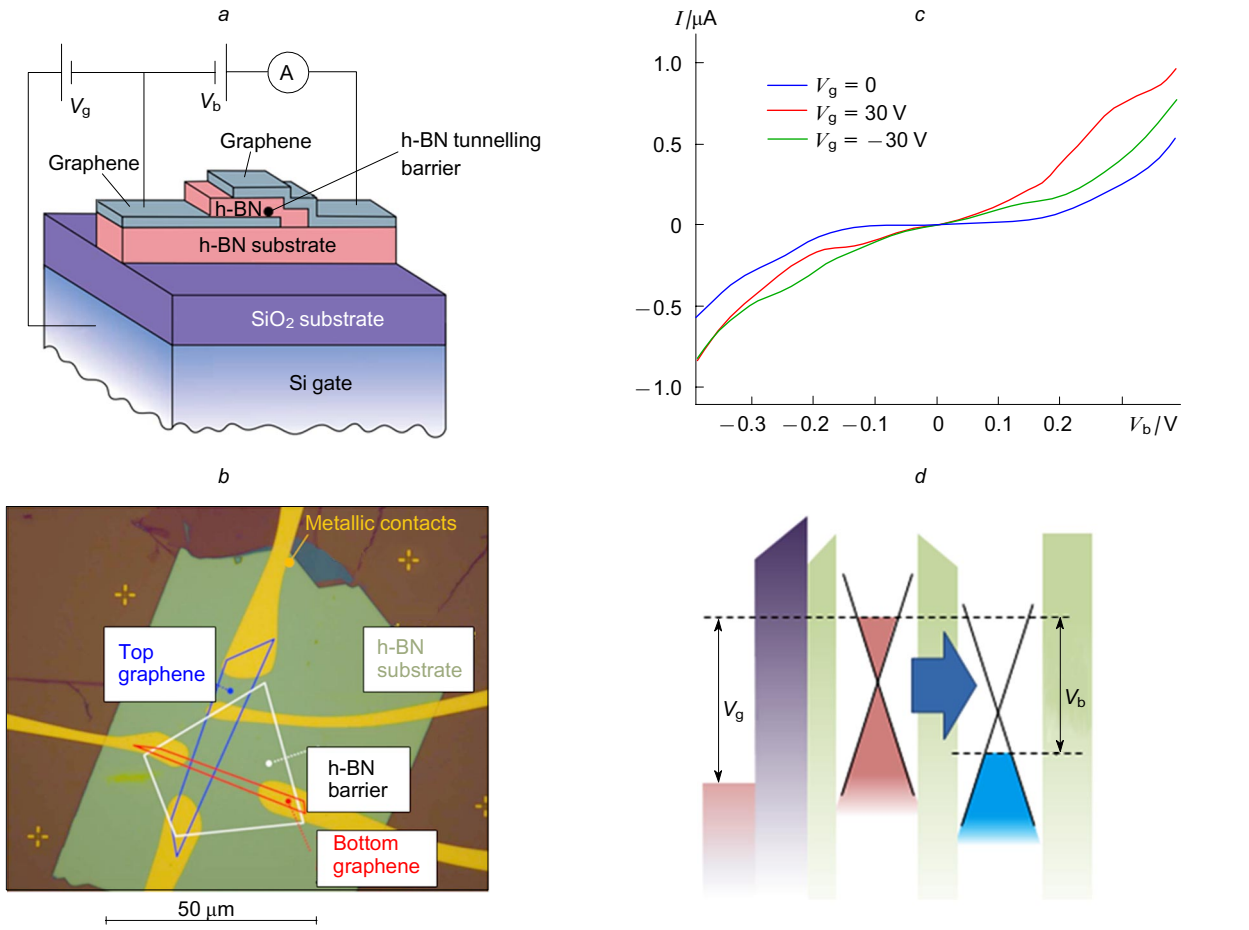


Figure 1. Schematic of experimental Gr/h-BN/Gr heterostructure (*a*); an optical micrograph of the experimental structure (*b*); tunnelling current I plotted *vs.* V_b at V_g = 0, 30 and −30 V (*c*); and schematic description of the influence of V_g and V_b on the filling of Dirac cones in graphene layers with charge carriers and on the tunnelling current (*d*).[15, 16]

In this case the tunnelling current is described by the expression

$$I(V) \propto \int \mathrm{d}E DoS_{\mathrm{b}}(E) DoS_{\mathrm{t}}(E - \mathrm{e}V) T(E) [f(E - \mathrm{e}V) - f(E)] \qquad (2)$$

Here DoS_i is the density of states in the layer, e is the electron charge, $T(E)$ is the dependence of structure transparency on the electron energy, and $f(E)$ is the Fermi distribution function.

Changes in the gate voltage V_{g} led to changes in the carrier concentration in the Gr layers (mainly in the lower layer) and in the tunnelling current (see Fig. 1 *c*). As mentioned above, the authors of the early studies ignored the role of the angular mismatch of layers in tunnelling; the understanding of this role and of the action mechanism of this parameter on tunnelling transitions came more recently.[14] The relation between angular misorientation and interlayer tunnelling was explained using the model shown in Fig. 2.

Since the Dirac cones arranged at the points K or K' at the boundary of the Brillouin zone, even a small angular mismatch between the crystal lattices of the Gr layers causes a large shift of the cones corresponding to each Gr layer in the k-space and, therefore, an abrupt decrease in the crossing lines of their surfaces, which determines the number of states accessible to interlayer tunnelling transitions with conservation of the momentum component aligned with the layers. As a result, at moderate carrier concentrations typical of most experiments, tunnelling with momentum conservation appears to be impossible without involvement of electron scattering by phonons or lattice defects. However, misoriented structures allowed one to study inelastic tunnelling transitions without momentum conservation involving phonons or localized states in the barrier layers.

Prior to going to the description of experiments on tunnelling in such systems, it is useful to consider specific features of electrostatic model of a graphene tunnelling transistor (Fig. 3 *a*) that are due to specific energy band structure of this material and to partial shielding of electric field gate near the electrical neutrality point.[15, 16] Within the framework of this model the relation between the chemical potentials, μ_i, of the layers, the charge carrier concentrations, n_i, and the voltages V_{g} and V_{b} is described by the following system of equations:

$$\mathrm{e}V_{\mathrm{b}} = \mu_{\mathrm{b}} - \mu_{\mathrm{t}} - \Delta\varphi \qquad (3)$$

$$\mathrm{e}V_{\mathrm{g}} = \mu_{\mathrm{b}} + \frac{\mathrm{e}^2 D(n_{\mathrm{b}} + n_{\mathrm{t}})}{\varepsilon\varepsilon_0} \qquad (4)$$

where D is the total thickness of the SiO_2 substrate and the h-BN sublayer, d is the thickness of the h-BN tunnelling barrier, the chemical potential of monolayer graphene is $\mu_i = \pm\hbar v_{\mathrm{F}}(\pi|n_i|)^{1/2}$, $\Delta\varphi = \mathrm{e}^2 d n_{\mathrm{t}}/\varepsilon\varepsilon_0$ is the energy difference between the electrical neutrality points of the upper and lower graphene layers, ε and ε_0 are the dielectric permittivity and absolute dielectric permittivity, respectively.

Solution to this system of equations gives the intersection points of the chemical potentials μ_i with the electrical neutrality points of the layers in the $V_{\mathrm{g}} - V_{\mathrm{b}}$ coordinates (they are shown as dashed lines in Fig. 3 *b*) in the tunnelling conductance map $\mathrm{d}I/\mathrm{d}V_{\mathrm{b}}$, which manifest themselves as lines of conductance minima. These solutions, exactly determined for each particular transistor with specified thicknesses of the dielectric layers D and d, serve a basis for further identification of any other features the tunnelling conductance maps.

Studies of inelastic tunnelling in misoriented heterosystems Gr/h-BN/Gr made it possible to determine the phonon density of states spectra of the constituent layers.[17] Experimental dependences of the conductance on V_{b} demonstrated certain features (Fig. 4 *a* – *c*) that can be described to a good accuracy by calculations that take into account the phonon density of states in the graphene and barrier monolayers and, therefore, characterize the contribution of inelastic tunnelling transitions to the tunnelling conductance. Such transitions are allowed only if the chemical potential difference between the lower and upper graphene layers exceeds the phonon energy (see Fig. 3 *a*), which in

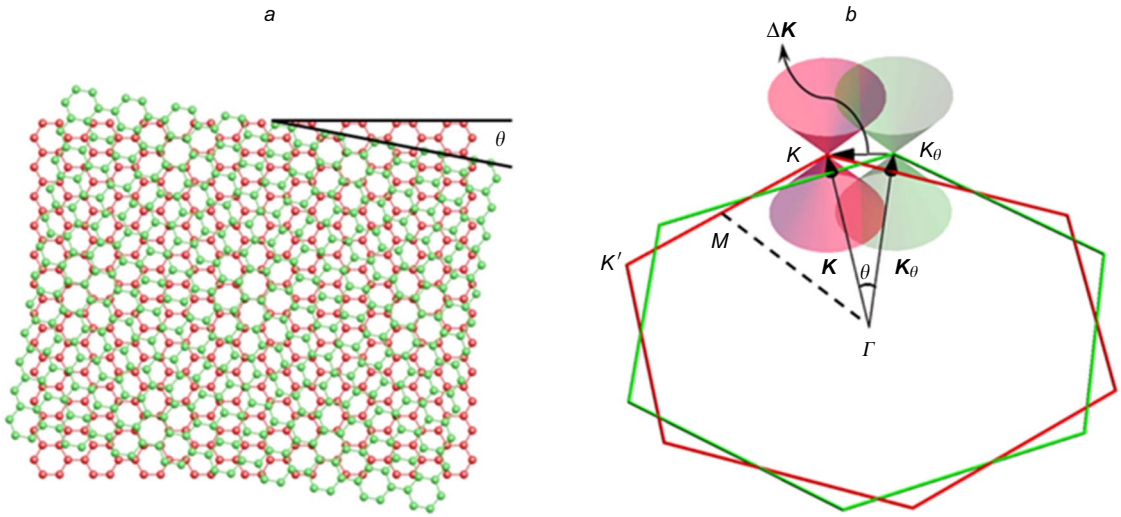


Figure 2. Schematic of twisted bilayer graphene with a twist angle θ between the upper and lower graphene lattices (*a*) and projection of this misorientation to the k-space (*b*). The h-BN barrier layer between the graphene electrodes is not shown.[14, 16]
The K and K_θ points correspond to the lower and upper graphene layer, respectively.

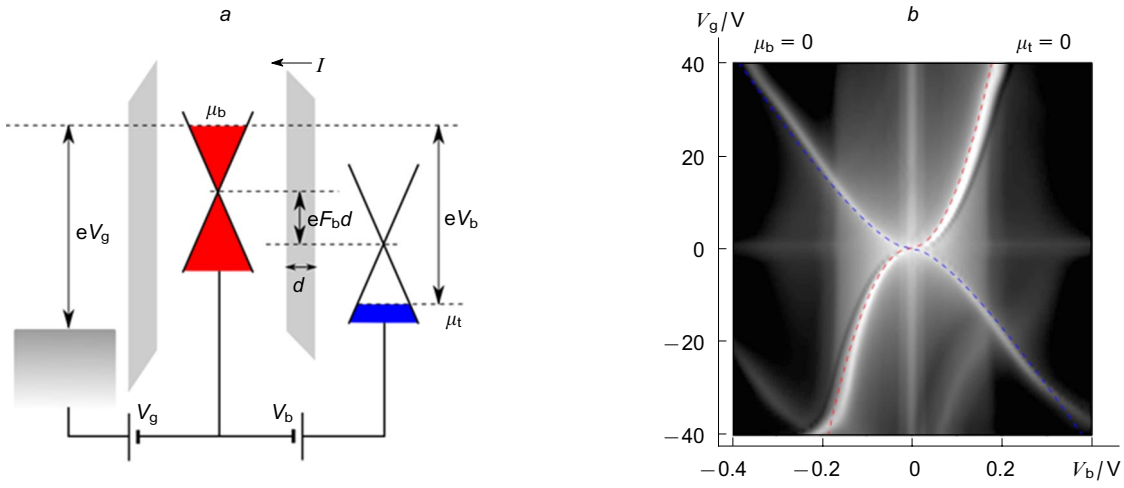


Figure 3. Energy band diagram for experimental heterosystem with a measurement circuit (*a*) and the corresponding conductance (dI/dV_b) map; dashed lines show the conductance minima for the case where the chemical potentials μ_t and μ_b are equal to the energies at the Dirac points in the upper and lower graphene layers (*b*).[16, 17] F_b is the electric field across the barrier.

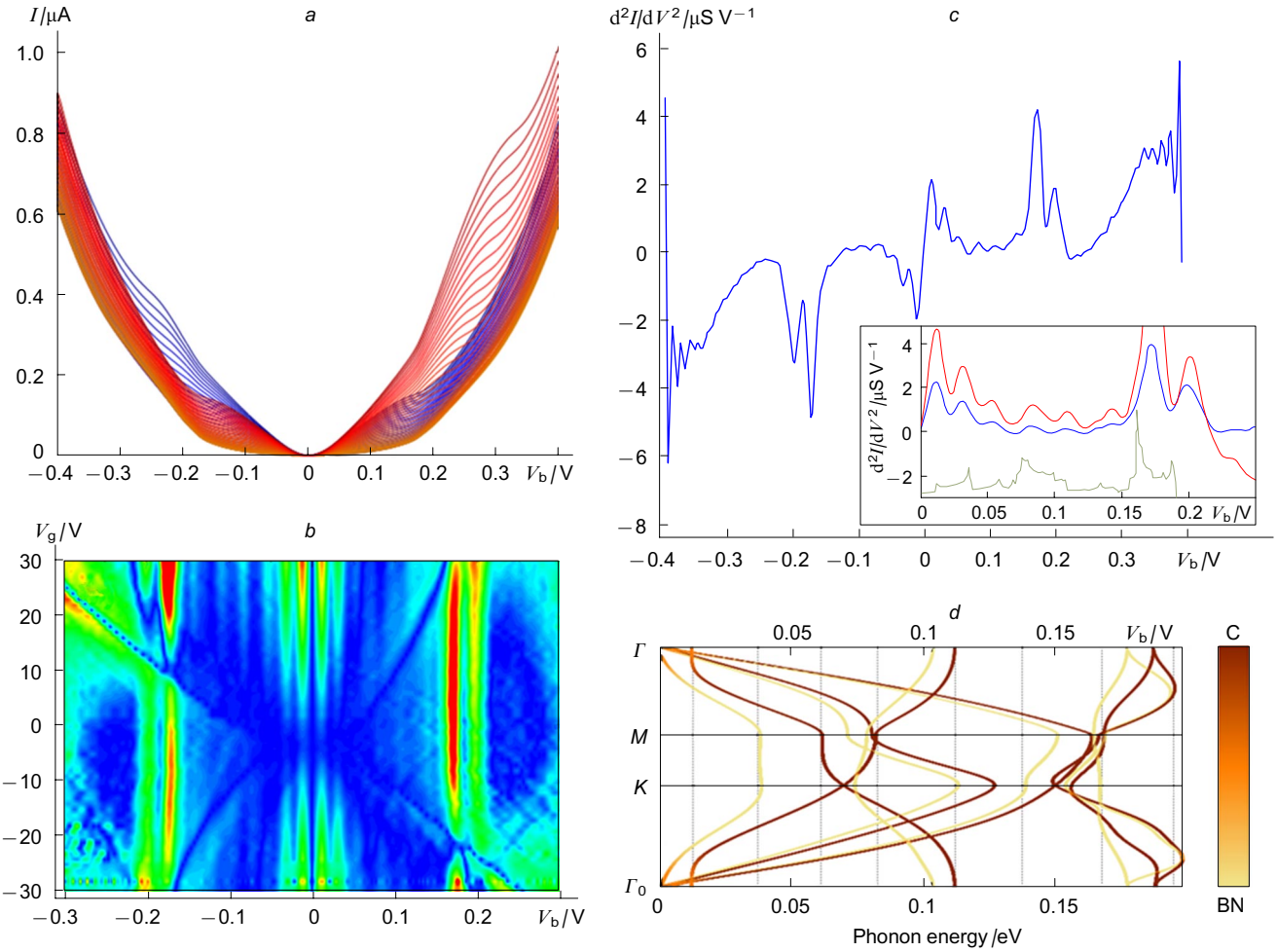


Figure 4. Results of experimental study of inelastic tunnelling in misoriented heterosystems Gr/h-BN/Gr: tunnelling characteristics of the device at different gate voltages (*a*), experimental conductance map (*b*), plots of conductance *vs.* V_b (*c*) and phonon dispersion of Gr/h-BN heterostructure (*d*). (Based on the data taken from Ref. 17).
(*a*) The gate voltage was varied from −30 (red lines) to 30 V (blue lines); (*b*) vertical lines in the map correspond to tunnelling transitions with emission of phonons; (*c*) blue lines denote averaged experimental dependences of conductance for all gate voltages, red line (see inset) is the experimental dependence of conductance at $V_g = 30$ V, green line (see inset) is the theoretical density of phonon states for monolayer graphene in the Gr/h-BN heterostructure.

turn corresponds to the bias voltage of a particular resonant conductance peak. A comparison of the phonon energies corresponding to the experimental resonances with the calculated one-phonon densities of states of monolayer graphene and bilayer system Gr/h-BN, as well as with the partial densities of phonon states mainly related to the motion of carbon, boron and nitrogen atoms showed that positions of the resonances are in good agreement with peaks in the theoretical curves and this gave a key to understanding the nature of the resonances observed (see Fig. 4 *c*,*d*).

Tunnelling involving localized states in van der Waals structures was first time studied [18, 19] in relation to metal/h-BN/metal and metal/h-BN/Gr systems in which series of tunnelling resonances in the experimental $I-V$ curves were explained by transitions through 0D states of defects in the crystal structure of the h-BN barrier. At present, it is assumed that localized electronic states can exist in the band gap of h-BN crystal due to the presence of intrinsic structural defects and impurities, in particular, different kinds of vacancies and inclusion atoms (most often, carbones) that are present in nominally pure h-BN crystal. Defects can also be introduced unintentionally during mechanical exfoliation of h-BN and incorporation into the multilayer van der Waals heterostructure. However, this assumption provides no explanation for experimentally observed large number of different levels in the band gap of h-BN and gives no way to describe their spectrum.

Resonant tunnelling between two monolayer graphene electrodes through localized states in the h-BN barrier was studied [20] using samples with one or two gates that controlled the concentrations and chemical potentials of charge carriers in the graphene layers. The results of measurements were used to determine the energies and spatial arrangement in the direction of tunnelling of each of more than 50 detected different localized intra-barrier states with an accuracy to a monolayer. Also, three-step electron tunnelling transitions through two spatially separated localized states were considered. The crystal lattices of graphene monolayers used as electrodes were misoriented to suppress direct inter-band resonant tunnelling with conservation of the momentum component aligned with the layers. This makes it possible to thoroughly study a small tunnelling

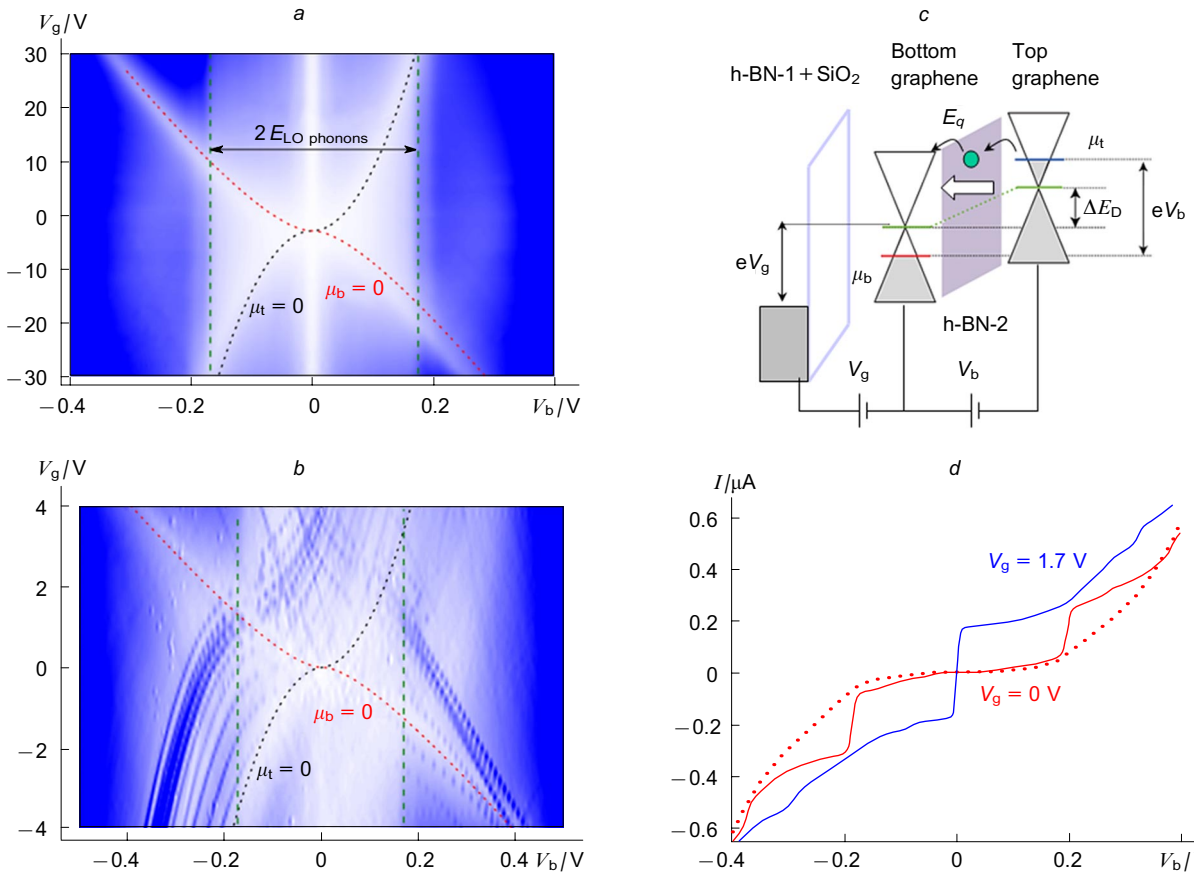


Figure 5. Results of experimental study of tunnelling transport in Gr/h-BN/Gr heterostructures with strongly misoriented graphene layers and different quality of h-BN layers: conductance maps of a perfect defect-free sample (*a*) and a sample with numerous defect states (*b*), schematic of a Gr/h-BN/Gr structure and tunnelling processes in it (*c*), and $I-V_b$ characteristics of this structure at $V_g = 0$ and 1.7 V.[21] (*a*) The red and black dotted lines are the calculated trajectories of the intersection points of the chemical potentials μ_t and μ of the upper and lower electrodes, respectively, with the electrical neutrality points; $E_{LO\ phonons}$ is the energy of optical phonon; (*b*) numerous dark-blue lines represent the motion of defect levels; *c*: shown is tunnelling through the defect-free regions of the structure (white arrow) and through the localized state in the barrier E_q (black arrows), ΔE_D is the energy shift of Dirac points, which depends on V_g and V_b; (*d*) the red dotted line is the $I-V_b$ characteristic of the defect-free sample with the same nominal structural parmeters at $V_g = 0$.

current during transitions through an individual localized state.

A systematic study of tunnelling transport in Gr/h-BN/Gr heterostructures with high degree of misorientation of graphene layers and different-quality h-BN layers (Fig. 5) was reported.[21] It involved experiments aimed at studying how defect states (from zero to several tens of defect levels in the band gap of h-BN) manifest themselves in tunnelling and how they are related to characteristic curves of the elecrostatic model for perfect defect-free heterostructure. The conductance map of the sample with numerous defect states in the h-BN tunnelling barrier (see Fig. 5 *b*) demonstrates numerous trajectories (dark narrow lines of conductance maxima) that correspond to the thresholds of tunnelling transitions through defect levels and pass nearly parallel to the characteristic curve $\mu_t = 0$. Emphasize that this systematic study of manifestation of defect states in tunnelling and their relation to the characteristic lines in the conductance maps of defect-free samples was carried out within a single series of experiments using one set of samples containing same-type h-BN layers.

Previously,[18,19] this relation was not observed. The critical effect of resonant tunnelling through localized states on the total transport, where the magnitude of the current jump much exceeds the non-resonant current through the h-BN barrier, was detected experimentally for only one sample (see Fig. 5 *d*). In zero magnetic field the $I-V_b$ curves (see Fig. 5 *d* and Fig. 6 *b*) demonstrated a step-like feature that transformed to a current peak followed by NDC region (blue curve in Fig. 6 *b*) in a magnetic field (B) of 4 T. This pattern iof the $I-V_b$ curve is due to simultaneous coincidence of the Landau levels in the graphene layers and in the defect level E_1 in the barrier (see Fig. 6 *a*). In essence, the resonant channel E_1 simultaneously acts as an amplifier of the tunnelling current and as a narrow probe of the density of states in the conductive layers that contribute to the total current.

It is just the situation where the resonant current through a single defect level dominates the entire range of experimental values of V_g and V_b, that allow one to experimentally study the density of states of graphene by scanning the material using the defect level. As a result, the density of states of graphene was studied in a magnetic field with such a sensitivity that made it possible to detect the splitting of the zeroth Landau level at $B \approx 4$ T upon removal of the spin and valley degeneracy. This in turn gives grounds to hope for feasibility of future experiments on the study of correlation features of the density of states of 2D conductive layers in van der Waals structures using the 0D state in semiconductor heterostructures as probe (similarly to the early studies [6,7]).

Unexpectedly, the presence of the NDC region in the experimental $I-V$ curve measured in magnetic field made it possible to observe generation of tunnelling current [21,22] (see inset in Fig. 6 *b*) at a frequency of 700 Hz. This value is most probably due to specific features of the interior of the heterostructure since it is basically different from the theoretical estimate (about 50 GHz) for similar structures.[13]

Earlier, both the NDC region and corresponding current generation during tunnelling between graphene layers with well-matched crystal lattices were observed in the $I-V$ curves;[14] however, current generation during magnetotunnelling through the 0D state level was observed neither in graphene nor in semiconductor structures. If different

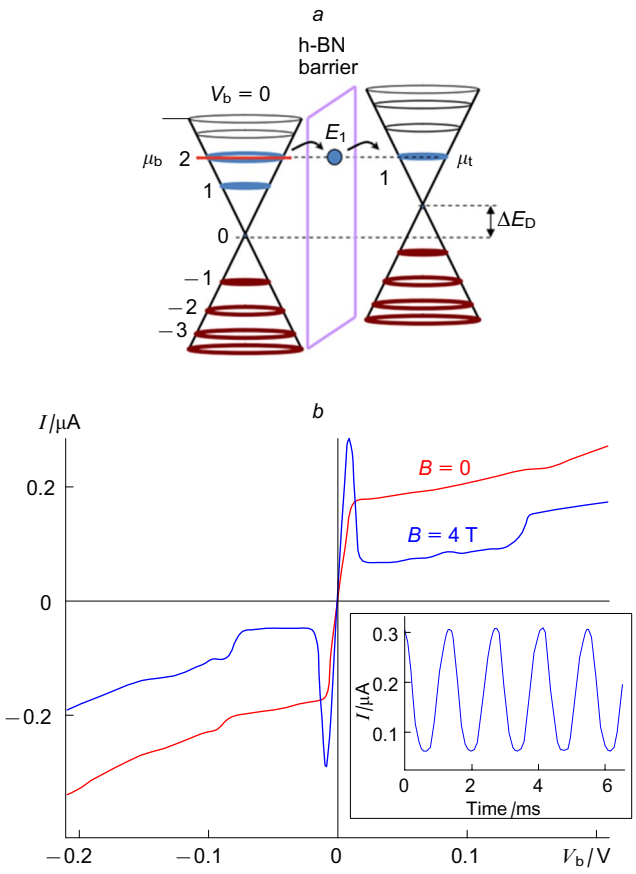


Figure 6. Schematic of tunnelling at $B = 4$ T and $V_b = 0$ (*a*) and $I-V_b$ characteristics in the region of tunnelling transition through the defect level E_1 in magnetic field $B = 4$ T, perpendicular to layers, and in the absence of magnetic field (*b*).[21,22]
(*a*) Numbers enumerate the Landau levels, ΔE_D is the energy shift of Dirac points; (*b*) the inset shows generation of tunnelling current in the resonance region.

barrier layers have two close-lying (in the direction perpendicular to tunnelling direction) states with slightly different energies, adjustment of positions of their levels until coincidence by varying the bias voltage will be followed by a sharp current peak in the $I-V$ curves even in the absence of magnetic field (Fig. 7).

As mentioned above, step-like features and peaks in the $I-V_b$ curve denoted by E_1 and $E_1 = E_2$ originate from tunnelling transitions between the source and drain in graphene through one or two defect levels in the barrier. A multiple increase in the resonant current during transitions through two levels compared to transition through one defect is due to natural increase in the tunnelling transparency of the system. Tunnelling involving one or two defect levels E_1 and E_2 is visualized in the insets in Fig. 7 where cones and parabolas correspond to the energy band structures of mono- and bilayer graphene. Clearly, the structures [22] cannot be used for practical applications owing to random appearance of localized intra-barrier states. Utilization of the 0D states in van der Waals heterostructures seems to be of considerable interest and the first attempt to fabricate such structures containing a layer of graphene quantum dots incorporated into the h-BN barrier was reported very recently.[23]

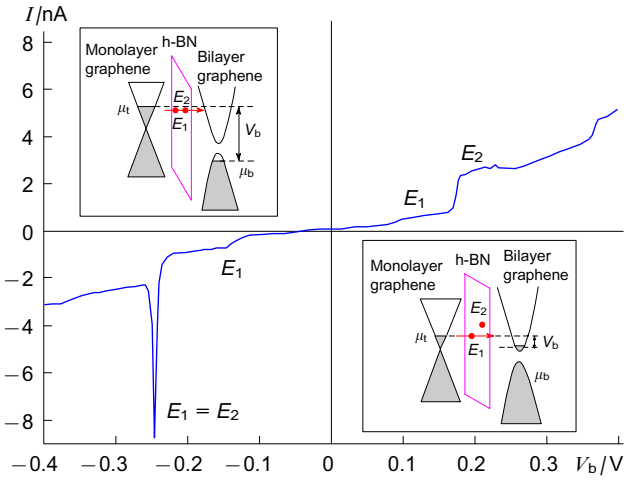


Figure 7. $I-V$ Curve for the sample with the top bilayer graphene electrode measured at 4.2 K. (The plot is based on the data taken from Ref. 22).
The steps and peaks denoted as E_1, E_2 and $E_1 = E_2$, characterize the tunnelling transitions between the source and drain through one or two defect levels in the barrier. Shown are schemes of tunnelling transitions involving one (lower inset) and two (upper inset) defect levels in the barrier.

Among numerous studies on tunnelling in misoriented structures, mention should be made of an experiment aimed at 'self-tuning' the orientations of two graphene sheets by heating.[16]

The experiment is essentially as follows. As mentioned above, the characteristic behaviour of the tunnelling conductance of the Gr/h-BN/Gr system (ignoring the phonon and other inelastic contributions) can be quite simply and unambiguously mapped onto a plane in the $V_b - V_g$ coordinates. Such a map is similar to that presented in Fig. 3 *b*. If the tunnelling system is composed of bilayer graphene sheets, parabolic energy band structures of these sheets cause significant changes in the characteristic map in the $V_b - V_g$ coordinates, and the lines corresponding to conductance minima will transform to straight lines that intersect at the origin. The experiment invloved measurements of the conductance map of the Gr/h-BN/Gr system that exactly matched the characteristic map (Fig. 8 *a*,*d*). Then, the upper graphene flake was covered with yet another flake with similar orientation of the crystal lattice (angular mismatch was about 5°) and the conductance map of the combined system Gr + Gr/h-BN/Gr was measured. The map looked as a set of highly blurred lines that could not be analytically described (see Fig. 8 *b*,*e*). However, annealing of the structure at 200 °C for 12 h led to the

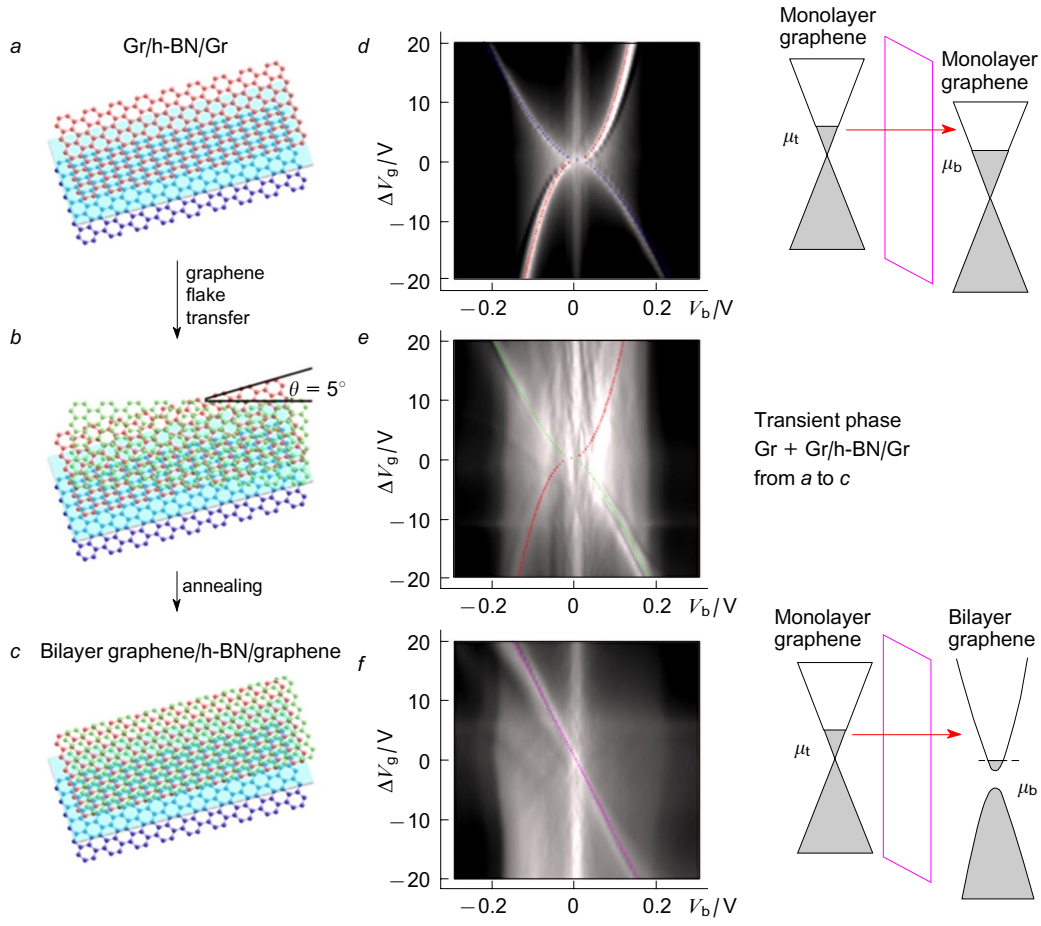


Figure 8. Evolution from monolayer graphene to twisted graphene layers and bilayer graphene ($a-c$), schematics of different graphene tunnelling transistors and the measured dI/dV conductance maps as functions of V_b and V_g for these devices ($d-f$).[16]
Dotted lines are the corresponding electrostatic calculations of the characteristic lines for zero chemical potentials.

appearance of well-defined straight lines in the conductance map and these lines were described using a modified system of equations (3), (4) assuming tunnelling from bilayer graphene to monolayer graphene (see Fig. 8 *c*, *f*). It follows that heating caused the crystal lattice of the upper graphene flake to change its spatial orientation relative to the crystal lattice of the lower graphene flake until a common bilayer graphene sheet is formed. The need for such a long-term annealing was due to the fact that the space between the upper graphene sheets was filled with numerous adsorbed molecules that precluded instantaneous spontaneous tuning of the crystal lattices. Based on the aforesaid, it was concluded that randomly oriented upper graphene flakes undergo transformation to bilayer graphene with parabolic energy dispersion. This conclusion was verified and confirmed by Raman spectroscopy.

3. Tunnelling with momentum conservation in van der Waals heterostructures with small angular mismatch of constituent layers

It was theoretically predicted[24] that tunnelling between perfecrty matched graphene layers should be accompanied by the appearance of a sharp resonant current peak in the $I-V$ curves, followed by an NDC region due to tunnelling transitions with conservation of both momentum and energy. Besides, it was demonstrated that tunnelling is strongly affected by the angular mismatch between the crystal lattices of the upper and lower graphene layers. It was shown that the resonant conductance is a sharp function of the misorientation angle between the crystal lattices of the upper and lower electrodes. As a result, misorientation of the crystal lattices even by a few tenth of a degree should lead to broadening of narrow and high conductance peaks for perfectly matched electrode lattices, while the peak current should decrease.

However, experimental verification of this prediction required considerable technological efforts. In graphene, charge carriers fill *K*-points of the Brillouin zone; therefore, the most difficult step in fabrication of the resonant tunnelling system Gr/barrier/Gr was to attain a sufficiently high degree of angular alignment of two layers of graphene electrodes. It was shown practically that an angular misalignment of a few degrees is sufficient for efficient suppression of resonant tunnelling with energy and momentum conservation. Initially, rotational alignment of graphene layers involved visual determination of straight edges of the graphene flakes being exfoliated followed by alignment of graphene layers during the transfer step in the hope that the edges chosen will have the same crystallographic orientation in both flakes. More recently, it was shown that thorough visually controlled mechanical alignment during the transfer step allows one to align graphene flakes to an accuracy of at most $1.5-2^{\circ}$.[14] Fabrication of Gr/barrier/Gr resonant van der Waals systems using polymeric hemispherical handles for transfer of graphene flakes improves the angular alignment to a value of 0.1°.[25]

The first experiment on observation of the NDC region during tunnelling in the van der Waals system Gr/barrier/Gr was reported in 2013.[26] Although the theoretical prediction[24] of the negative effect of angular mismatch (see above) was known at that time, experimental data were interpreted using a model that assumed scattering by a specific (exotic) bell-shaped potential as the main reason for the presence of the NDS region and ignored the negative effect of misorientation on the resonance.

The view of resonant tunnelling in the structures in question was revised in the next study.[14] In essence, the aim of that work was to confirm the concept of resonant tunnelling in Gr/barrier/Gr van der Waals systems reported in theoretical studies.[24, 27] The angular alignment achieved in the first experiment[26] was high enough to observe the NDC region; however, this probably occurred by chance. That is why Mishchenko *et al.*[14] paid particular attention to this issue and also proposed a method for angular alignment of crystal lattices with an accuracy to $1-2^{\circ}$; this technique was used to fabricate experimental tunnelling structures based on graphene and boron nitride.

In the experimental system, the tunnelling current between graphene layers was controlled by the bias voltage between these layers and by the voltage applied to the underlying doped silicon electrode acting as gate. Experimental results confirmed the fact that the tunnelling conductance of such heterostructures depends critically on the relative orientation of the crystal lattices of the constituent atomic layers owing to the influence of the selection rule for conservation of intra-layer momenta of tunnelling electrons. The reason for such a strong dependence is that misorientation of two graphene lattices by merely a few degrees leads to large displacement of the corresponding Dirac cones in the momentum space (see Figs 2 and 9 *a*). The current between the graphene electrodes is determined by the probability of electron tunnelling transitions, which depends on the length of the intersection line of Dirac cones of adjacent graphene layers. Mutual arrangement of the Dirac cones depends on the misorientation alignment angle between the crystal lattices of graphene layers and can be controlled through the voltage V_b. The degree of intersection of the Dirac cones is maximum in a narrow range of V_b values. Thus, the $I-V$ curves will exhibit a resonance peak and an NDC region. The results of theoretical simulation of the operation of such a transistor were in excellent agreement with the experimental $I-V$ curves and revealed characteristic features due to coincidence of the Dirac point in one graphene layer with band edges or with the Dirac point of the other graphene layer.

In addition to demonstration of resonant tunnelling, it was shown how the energy band structure of one graphene layer can be efficiently shifted (in the momentum space) relative to that of the other layer by e*Bd*, where *d* is the tunnelling path length, under the action of the Lorentz force in a magnetic field of up to $B = 15$ T applied parallel to the graphene layer (perpendicular to the tunnelling current flow in the sample). This will change the shape of the resonance and, as a consequence, the sharpness of the corresponding current peak. According to calculations, the resonance peak should split into six components upon removal of equivalence of the resonance conditions for all six pairs of Dirac cones of the two graphene layers. However, no splitting was observed in the experiments, probably, due to broadening of the resonance peaks. Such a splitting was detected in a more recent experiment with similar structures in a magnetic field of up to 30 T.[28] In addition, it was shown[28] that rotation of the applied magnetic field vector in the plane of the sample led to periodic changes in the resonance conditions for all six pairs of Dirac cones at the corners of the Brillouin zone and that the V_b voltage corresponding to the resonance at each corner is a sinusoidal function of the

angle between the magnetic field direction and the specified crystallographic direction of the graphene lattice. In contrast to similar experiments on tunnelling in other 2D semiconductor systems,[29] in this case agreement between the experimental amplitudes of the partial resonances and the results of calculations was achieved taking into account the chiral nature of the wave functions, which is due to the existence of two sublattices in the crystal structure of graphene. A direct comparison of experimental data with the results of calculations carried out both with inclusion of and ignoring the chiral nature of the wave functions revealed better agreement in the former case. Based on this fact, it was concluded that chirality is preserved during tunnelling. The need to account for chirality during magnetotunnelling in parallel 2D electronic systems was theoretically predicted elsewhere.[30]

4. Van der Waals heterostructures in a magnetic field perpendicular to layers. Tunnelling transitions between Landau levels in graphene layers

Tunnelling in a magnetic field perpendicular to graphene layers was for the first time experimentally studied in one-gate tunnelling structures composed of two monolayer graphene sheets separated by a h-BN barrier; the role of the lower gate was played by the heavily doped Si substrate.[31] In this case the magnetic field quantizes (i) the in-plane motion of electrons and (ii) the electron energies into spectra of non-equidistant discrete Landau levels since the properties of massless Dirac fermions in graphene are fundamentally different from those of charge carriers in traditional materials. The Landau levels can be graphically represented as circles on the surface of Dirac cones (Fig. 9 *b*) whose energy spectrum is given by

$$E = \pm v_F(2e\hbar|N|B)^{1/2} \qquad (5)$$

where $N = 0 \pm 1 \pm 2$ and v_F is the Fermi velocity. The eigenstates of electrons on the Landau levels in graphene are composed of two components, one of the pseudospin origin and the other originating from states similar to those of a simple harmonic oscillator.

The authors of Ref. 31 revealed sets of resonant features of tunnelling spectra, which corresponded to tunnelling transitions of electrons between Landau levels in two graphene layers, *viz.*, the tunnelling current maxima corresponded to the coincidence of filled and empty Landau levels in the emitter and collector, respectively. Changes in the filling of the Landau levels in the graphene layers were achieved by varying the gate voltage V_g. Three-dimensional tunnelling conductance maps constructed in the $V_b - V_g$ coordinates exhibited regions of tunnelling transitions between different sets of Landau levels in the emitter and collector representing the total tunnelling current at each point of the map. Each conductance region in the map corresponds to certain sets of filled and empty Landau levels in two graphene layers that are involved in tunnelling transitions and contribute to the tunnelling current. Features of the map were identified based on the results of numerical calculations carried out considering the contributions of all Landau levels in two graphene layers that were simultaneously in resonance in the tunnelling conductance window, *i.e.*, in the energy interval between the Fermi

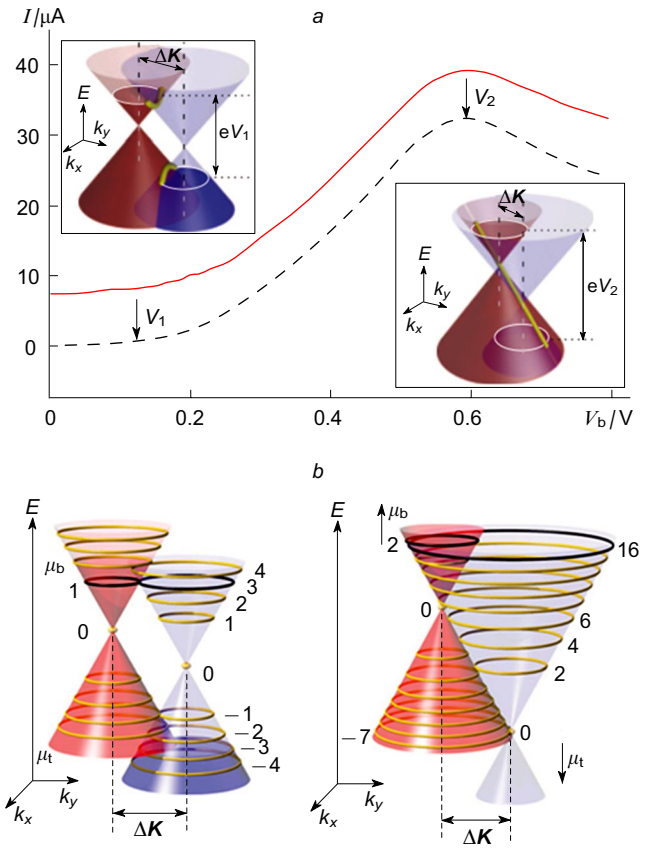


Figure 9. Experimental $I-V$ curves for Gr/h-BN/Gr tunnelling structure at $V_g = 0$, $B = 0$ T and $V_g = 0$, $B = 4$ T (dashed and solid lines, respectively) and a small angular lattice mismatch $\theta = 18°$ (*a*) and schematic representation of layer-by-layer tunnelling under Landau quantization conditions assuming wide tunnelling conductance window (*b*).[16]
(*a*) The insets show the intersections of the Dirac cones with the upper (blue) and lower (red) graphene layers, which correspond to the tunnelling threshold at V_1 and to the current peak at V_2 (arrowed) in the $I-V$ curves.

levels of the emitter and collector graphene layers involved in the tunnelling process. Just those filled and empty parts that could directly participate in tunnelling transitions were 'cut' by the conductance window from the density of states of each layer. The experiment was complicated by the presence of only one gate, which led to the need to apply high bias voltages V_b, *i.e.*, to use a 'wide tunnelling conductance window' where several pairs of Landau levels with equal energies in each of the graphene layers were simultaneously involved in tunnelling. The results of calculations appeared to be in good agreement with the experimental conductance maps and even allowed the authors to conclude that energy, momentum and chirality are conserved in tunnelling processes. However, in order to unambiguously identify and describe tunnelling transitions between Landau levels and to soundly discuss the degree of fulfillment of conservation laws, it would be much more convenient to consider double-gate structures that enable independent control of the carrier concentration in each graphene layer. Similar structures based on GaAs were

successfully used to study equilibrium tunnelling between 2D electronic systems in a narrow conductance window.[32, 33] When applied to tunnelling graphene heterostructures, this approach made possible the selective study of tunnelling between individual Landau levels from each layer, cut by the narrow conductance window, and fundamentally simplified the interpretation of experimental results.

Magnetotunnelling studies in narrow conductance window in double-gate Gr/h-BN/Gr structures were reported.[34, 35] Three-dimensional equilibrium tunnelling conductance maps were constructed in the $V_b - V_g$ coordinates and identified. These maps characterize the motion of resonances between dufferent combinations of individual Landau levels in the upper and lower graphene layers. Magnetotunnelling spectroscopy of transitions between Landau levels in such a double-gate structure under equilibrium conductance conditions not only allows one to aviod numerical calculations in order to identify transitions, but also provides unambiguous information on broadening of the Landau levels and on the properties of the wave functions, *e.g.*, on the role of chirality at tunnelling. Transitions between split Landau levels with different indices from different graphene layers were observed in strong magnetic field ($B > 8$ T) owing to removal of the spin and valley degeneracy (Fig. 10).

An unexpectedly detected increase in the experimental interlayer tunnelling conductance for transitions between Landau levels in strong magnetic fields with increasing temperature (Fig. 11) was not explained within the framework of the one-electron concept; presumably, this can indicate manifestation of a Coulomb gap at tunnelling.[32, 33, 36, 37] It follows that many-body correlation interactions should be included in consideration; however, this requires additional experimental and theoretical studies.

Although it is widely believed that the existence of Wigner crystal in graphene in zero magnetic field is impossible (see, *e.g.*, Refs 38 and 39), the possibility for such a crystal to exist in nonzero magnetic field was theoretically predicted more than a decade ago and various crystalline phases of this system were described.[40] Therefore, there is still hope for the detection of Wigner crystallization effects in graphene systems as a tunnelling Coulomb gap in a magnetic field and as other, more subtle many-body effects, *e.g.*, 'excitonic contribution' to the tunnelling gap, which is due to attraction of an electron tunnelling from the correlated system to a slowly relaxing hole that appeared at the site just left by the electron.

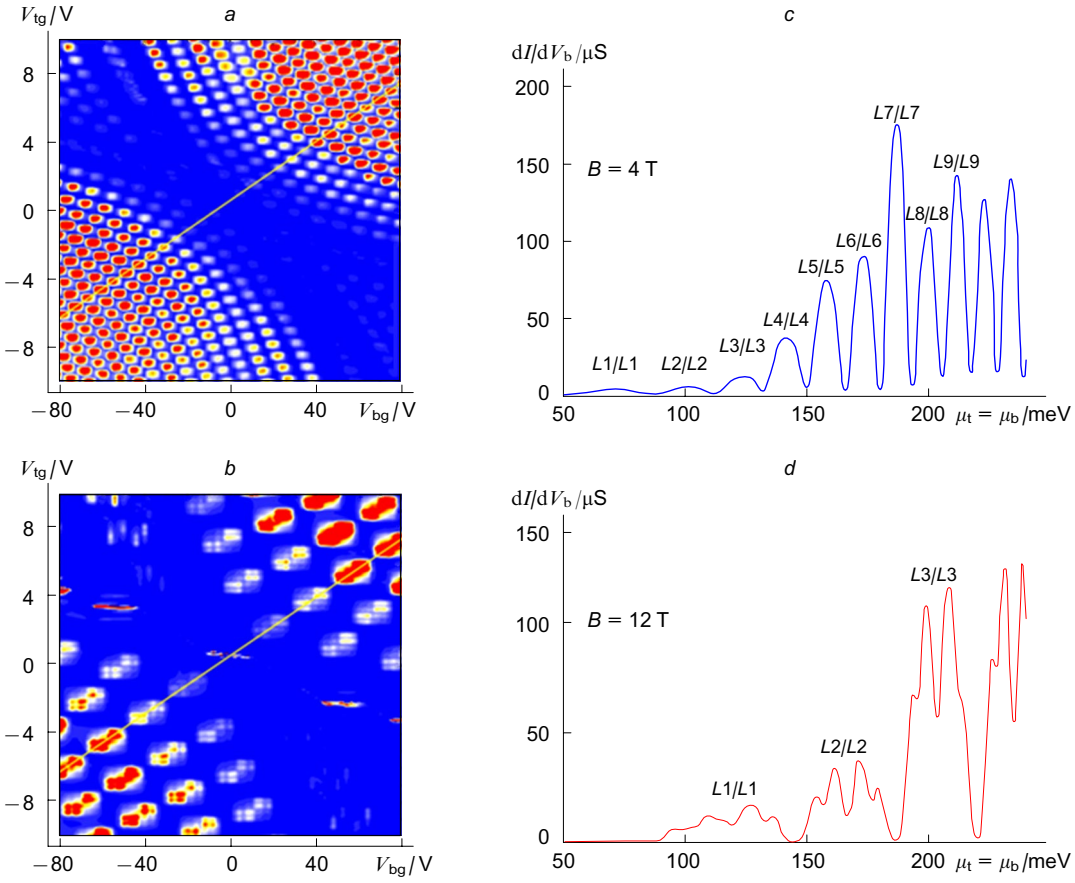


Figure 10. Equilibrium tunnelling conductance maps at $T = 2$ K and $B = 4$ (*a*), 12 T (*b*) and their cross-sections (*c*, *d*).[35]
Lines in Figs *a*, *b* correspond to the condition of equal carrier concentrations in the upper and lower graphene layers, $n_t = n_b$; Figs *c* and *d* represent the corresponding cross-sections of the equilibrium conductance maps. Figure *d* shows a quadruplet splitting of each resonance peak from Fig. *c* owing to removal of degeneracy.
V_{bg} and V_{tg} are the lower and upper gate voltages, respectively; *LN*/*LM* are transitions between Landau levels.

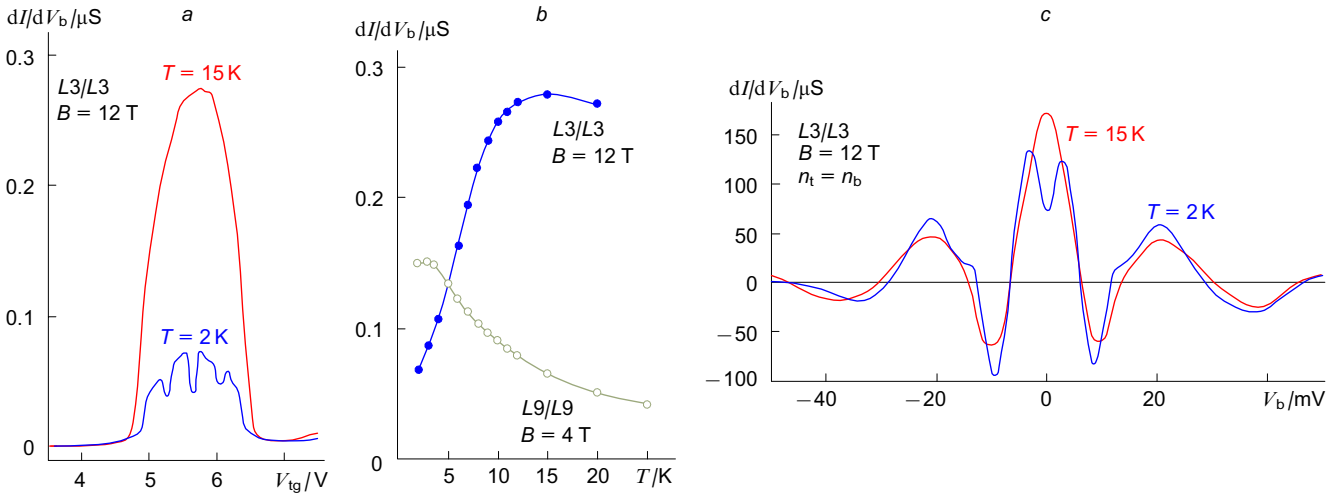


Figure 11. Tunnelling conductance dI/dV_b plotted *vs.* V_{tg} for the $L3/L3$ transition in the magnetic field $B = 12$ T at $V_{bg} = 57$ V, $T = 2$ (blue line) and 15 K (red line) (*a*); temperature dependences of the tunnelling conductance dI/dV_b at $V_{bg} = 57$ V and $V_{tg} = 5.4$ V at $B = 4$ (green line) and 12 T (blue line) (*b*); and suppression of the tunnelling conductance at $V_b = 0$ (*c*).[35]

* * *

In spite of brevity of this review, the authors hope that they clearly presented certain most interesting physical results of modern tunnelling spectroscopy studies of van der Waals heterostructures and the material can be useful to specialists working in related fields and to a wide circle of researchers as an introduction to the title field.

The illustrative material presented in the review was taken from different sources (references are specified in the text) and supplemented.

The work of E.E.Vdovin and Yu.N.Khanin was financially supported within the framework of the State Assignment No. 075-00475-19-00. The authors express their gratitude to Doctor of Sciences (Physics and Mathematics) S.V.Morozov for helpful discussions in the course of preparation of the manuscript.

References

1. E.L.Wolf. *Principles of Electron Tunneling Spectroscopy*. (New York: Oxford University Press, 1985)
2. R.K.Hayden, D.K.Maude, L.Eaves, E.C.Valadares, M.Henini, F.W.Sheard, O.H.Hughes, J.C.Portal, L.Cury. *Phys. Rev. Lett.*, **66**, 1749 (1991)
3. J.Smoliner, W.Demmerle, G.Berthold, E.Gornik, G.Weimann, W.Schlapp. *Phys. Rev. Lett.*, **63**, 2116 (1989)
4. J.Wang, P.H.Beton, N.Mori, L.Eaves, H.Buhmann, L.Mansouri, P.C.Main, T.J.Foster, M.Henini. *Phys. Rev. Lett.*, **73**, 1146 (1994)
5. E.E.Vdovin, A. Levin, A. Patan, L.Eaves, P.C.Main, Y.N.Khanin, Y.V.Dubrovskii, M.Henini, G.Hill. *Science*, **290**, 122 (2000)
6. A.K.Geim, P.C.Main, N.La Scala Jr., L.Eaves, T.J.Foster, P.H.Beton, J.W.Sakai, F.W.Sheard, M.Henini, G.Hill, M.A.Pate. *Phys. Rev. Lett.*, **72**, 2061 (1994)
7. P.C.Main, A.S.G.Thornton, R.J.A.Hill, S.T.Stoddart, T.Ihn, L.Eaves, K.A.Benedict, M.Henini. *Phys. Rev. Lett.*, **84**, 729 (2000)
8. A.A.Shashkin, S.V.Kravchenko. In *Strongly Correlated Electrons in Two Dimensions*. (Ed. S.V.Kravchenko). (Pan Stanford Publishing Pte Ltd., 2017). P. 47
9. I.E.Itskevich, T.Ihn, A.Thornton, M.Henini, T.J.Foster, P.Moriarty, A.Nogaret, P.H.Beton, L.Eaves, P.C.Main. *Phys. Rev. B*, **54**, 16401 (1996)
10. E.E.Vdovin, Yu.N.Khanin. *JETP Lett.*, **108**, 641 (2018)
11. A.H.Castro Neto, F.Guinea, N.M.Peres, K.S.Novoselov, A.K.Geim. *Rev. Mod. Phys.*, **81**, 109 (2009)
12. S.Kang, X.Mou, B. Fallahazad, N.Prasad, X.Wu, A.Valsaraj, H.C.P.Movva, K.Kim, E.Tutuc, L.F.Register, S.K.Banerjee. *J. Phys. D: Appl. Phys.*, **50**, 383002 (2017)
13. J.Gaskell, L.Eaves, K.S.Novoselov, A.Mishchenko, A.K.Geim, T.M.Fromhold, M.T.Greenaway. *Appl. Phys. Lett.*, **107**, 103105 (2015)
14. A.Mishchenko, J.S.Tu, Y.Cao, R.V.Gorbachev, J.R.Wallbank, M.T.Greenaway, V.E.Morozov, S.V.Morozov, M.J.Zhu, S.L.Wong, F.Withers, C.R.Woods, Y.-J.Kim, K.Watanabe, T.Taniguchi, E.E.Vdovin, O.Makarovsky, T.M.Fromhold, V.I.Fal'ko, A.K.Geim, L.Eaves, K.S.Novoselov. *Nat. Nanotechnol.*, **9**, 808 (2014)
15. L.Britnell, R.V.Gorbachev, R.Jalil, B.D.Belle, F.Schedin, A.Mishchenko, T.Georgiou, M.I.Katsnelson, L.Eaves, S.V.Morozov, N.M.Peres, J.Leist, A.K.Geim, K.S.Novoselov, L.A.Ponomarenko. *Science*, **335**, 947 (2012)
16. M.Zhu, D.Ghazaryan, S.-K.Son, C.R.Woods, A.Misra, L.He, T.Taniguchi, K.Watanabe, K.Novoselov, Y.Cao, A.Mishchenko. *2D Materials*, **4**, 011013 (2017)
17. E.E.Vdovin, A.Mishchenko, M.T.Greenaway, M.J.Zhu, D.Ghazaryan, A.Misra, Y.Cao, S.V.Morozov, O.Makarovsky, T.M.Fromhold, A.Patanè, G.J.Slotman, M.I.Katsnelson, A.K.Geim, K.S.Novoselov, L.Eaves. *Phys. Rev. Lett.*, **116**, 186603 (2016)
18. U.Chandni, K.Watanabe, T.Taniguchi, J.P.Eisenstein. *Nano Lett.*, **15**, 7329 (2015)
19. U.Chandni, K.Watanabe, T.Taniguchi, J.P.Eisenstein. *Nano Lett.*, **16**, 7982 (2016)
20. M.T.Greenaway, E.E.Vdovin, D.Ghazaryan, A.Misra, A.Mishchenko, Y.Cao, Z. Wang, J.R.Wallbank, M.Holwill, Yu.N.Khanin, S.V.Morozov, K.Watanabe, T.Taniguchi, O.Makarovsky, T.M.Fromhold, A.Patanè, A.K.Geim, V.I.Fal'ko, K.S.Novoselov, L.Eaves. *Commun. Phys. 1*, Art. No. 94 (2018)
21. Yu.N.Khanin, E.E.Vdovin, M.V.Grigor'ev, O.Makarovsky, M.Alhazmi, S.V.Morozov, A.Mishchenko, K.S.Novoselov. *JETP Lett*, **109**, 482 (2019)

22. Yu.N.Khanin, E.E.Vdovin, A.Mishchenko, K.S.Novoselov. *Semiconductors*, **53**, 1038 (2019)
23. G.Kim, S.Kim, J.Jeon, S.Yoon, S.Hong, Y.J.Cho, A.Misra, S.Ozdemir, J.Yin, D.Ghazaryan, M.Holwill, A.Mishchenko, D.V.Andreeva, Y.Kim, H.Y.Jeong, A.Jang, H.Chung, A.K.Geim, K.S.Novoselov, B. Sohn, H.S.Shin. *Nat. Commun.*, **10**, 230 (2019)
24. R.M.Feenstra, D.Jena, G.Gu. *J. Appl. Phys.*, **111**, 043711 (2012)
25. K.Kim, M.Yankowitz, B.Fallahazad, S.Kang, H.C.P.Movva, S.Huang, S.Larentis, C.M.Corbet, T.Taniguchi, K.Watanabe, S.K.Banerjee, B.J.LeRoy, E.Tutuc. *Nano Lett.*, **16**, 1989 (2016)
26. L.Britnell, R.V.Gorbachev, A.K.Geim, L.A.Ponomarenko, A.Mishchenko, M.T.Greenaway, T.M.Fromhold, K.S.Novoselov, L.Eaves. *Nat. Commun.*, **4**, 1794 (2013)
27. L.Brey. *Phys. Rev. Appl.*, **2**, 014003 (2014)
28. J.R.Wallbank, D.Ghazaryan, A.Misra, Y.Cao, J.S.Tu, B.A.Piot, M.Potemski, S.Pezzini, S.Wiedmann, U.Zeitler, T.L.M.Lane, S.V.Morozov, M.T.Greenaway, L.Eaves, A.K.Geim, V.I.Fal'ko, K.S.Novoselov, A.Mishchenko. *Science*, **353**, 575 (2016)
29. J.P.Eisenstein, T.J.Gramila, L.N.Pfeiffer, K.W.West. *Phys. Rev. B*, **44**, 6511 (1991)
30. L.Pratley, U.Zülicke. *Phys. Rev. B*, **88**, 245412 (2013)
31. M.T.Greenaway, E.E.Vdovin, A.Mishchenko, O.Makarovsky, A.Patane, J.R.Wallbank, Y.Cao, A.V.Kretinin, M.J.Zhu, S.V.Morozov, V.I.Fal'ko, K.S.Novoselov, A.K.Geim, T.M.Fromhold, L.Eaves. *Nat. Phys.*, **11**, 1057 (2015)
32. J.P.Eisenshtein, L.N.Pfeiffer, K.W.West. *Phys. Rev. Lett.*, **69**, 3804 (1992)
33. N.Turner, J.T.Nicholls, E.H.Linfield, K.M.Brown, G.A.Jones, D.A.Ritchie. *Phys. Rev. B*, **54**, 10614 (1996)
34. Yu.N.Khanin, E.E.Vdovin, A.Mishchenko, J.S.Tu, A.Kozikov, R.V.Gorbachev, K.S.Novoselov. *JETP Lett.*, **104**, 334 (2016)
35. Yu.N.Khanin, E.E.Vdovin, I.A.Larkin, O.Makarovsky, Y.A.Sklyueva, A.Mishchenko, Y.B.Wang, A.Kozikov, R.V.Gorbachev, K.S.Novoselov. *JETP Lett.*, **107**, 238 (2018)
36. E.V.Deviatov, A.A.Shashkin, V.T.Dolgopolov, W.Hansen, M.Holland. *Phys. Rev. B*, **61**, 2939 (2000)
37. I.N.Kotel'nikov, S.E.Dizhur, E.N.Morozova, E.V.Devyatov, V.T.Dolgopolov. *JETP Lett.*, **96**, 577 (2013)
38. H.P.Dahal, Y.N.Jogekar, K.S.Bedell, A.V.Balatsky. *Phys. Rev. B*, **74**, 233405 (2006)
39. V.T.Dolgopolov. *Phys. Uspekhi*, **60**, 731 (2017)
40. C.-H.Zhang, Y.N.Joglekar. *Phys. Rev. B*, **75**, 245414 (2007)